Received 20 November 2023; revised 3 February 2024 and 18 April 2024; accepted 1 May 2024. Date of publication 10 May 2024; date of current version 28 May 2024. The review of this article was arranged by Editor M. T. A. Rahimo.

Digital Object Identifier 10.1109/JEDS.2024.3399554

An Online Monitoring Method for Bond Wire Fatigue in IGBT Module

HONGTAO LIU (Student Member, IEEE), FEI WANG (Senior Member, IEEE), XIAOKANG ZHANG (Member, IEEE), WEIYI XIA (Student Member, IEEE), AND LINTAO REN (Member, IEEE)

School of Mechatronics Engineering and Automation, Shanghai University, Shanghai 200444, China

CORRESPONDING AUTHOR: F. WANG (e-mail: f.wang@shu.edu.cn)

This work was supported in part by the National Natural Science Foundation of China under Grant 52377193, and in part by the Program of Shanghai Academic Research Leader under Grant 23XD1421100.

ABSTRACT IGBT modules are core components of power electronic converters, and their reliability has gained significant attention. Among various reliability concerns, bond wire fatigue is a prominent issue. Bond wire fatigue can alter the electrical characteristics of IGBT modules, affecting the turn-off process of the IGBT. Consequently, it leads to changes in the collector-emitter voltage spike and the auxiliary emitter-emitter voltage spike during the turn-off process. The paper proposes the utilization of the K factor parameter which is not affected by the collector current and junction temperature, based on the collector-emitter voltage spike and the auxiliary emitter-emitter voltage spike, for bond wire fatigue monitoring of IGBT modules. Additionally, the monitoring of bond wire fatigue and junction temperature of IGBT modules was achieved based on the K factor parameter and the auxiliary emitter-emitter voltage spike. This provides a basis for the reliability assessment of IGBT modules.

INDEX TERMS IGBT module, bond wire fatigue, K factor, junction temperature extraction.

I. INTRODUCTION

IGBT (Insulated Gate Bipolar Transistor) module holds unique advantages in terms of large capacity, high performance, and cost-effectiveness. This provides ample justification for the widespread application of IGBT module. Such as renewable energy generation, high-voltage direct current transmission, energy storage, and electric power drive, among others. According to an industrial survey, power device failures account for 34% of the failures in power electronic converters [1]. Therefore, the reliability issues of power devices represented by IGBT module have become a focus of attention and research. Research has shown that the aging and failure of module packaging are the primary manifestation of IGBT module reliability issues. In the aging and failure of IGBT module packaging, bond wire fatigue is among the important types [2], [3], [4]. Caused by the difference in the coefficient of thermal expansion (CTE) between the chip and bond wire materials, the junction temperature fluctuation can cause thermal stress at the heel of the bond wire, resulting in fatigue of the bond wire [5]. Furthermore, the bond wire fatigue can affect the conduction loss and switching loss of IGBT, which further accelerates the aging process of bond wire. The bond wire fatigue occurs inside the module, which adversely affects the thermal and electrical characteristics of the IGBT module [6], [7], [8]. Existing bond wire fatigue detection methods can be divided into two main categories: active detection and passive detection methods [8]. Active detection is achieved by transmitting detection signals, such as ultrasonic waves, high-frequency electrical signals, etc., to the IGBT module to detect bond wire fatigue [9], [10], [11], [12]. However, the complex detection device limits the application of this method. Thus, the passive detection has become the main detection method of bond wire fatigue [13], [14].

Reference [15] uses a constant current source to charge the gate and uses the charging time as the detection parameter of bond wire fatigue. Nevertheless, this method has low sensitivity and is prone to causing IGBT to be mistakenly turned on. References [16] and [17] respectively

© 2024 The Authors. This work is licensed under a Creative Commons Attribution 4.0 License.
For more information, see https://creativecommons.org/licenses/by/4.0/

use gate overvoltage during the turn-on process and gate reverse overvoltage during the turn-off process as detection parameters for bond wire fatigue. Due to the susceptibility of gate voltage interference and low sensitivity during the switching process, it cannot be applied to online detection of IGBTs. References [18] and [19] respectively use the overvoltage of the collector-emitter during the turn on and turn off processes as the detection parameter of bond wire fatigue. It should be noted that this method detects the bond wire status of other IGBTs with the same bridge arm, which is unfavorable for the current bond wire status detection of IGBTs. Moreover, the inductance of the bond wire is relatively small compared to external parasitic inductance, and the sensitivity of these detection parameters is also not high. References [20] and [21] use the changes in collector saturation current and short-circuit current as detection parameters of bond wire fatigue. However, the saturation current and short-circuit current are very high. Even though these methods have high sensitivity and anti-interference capabilities, their implementation is difficult and can cause irreversible damage to the module. Reference [22] obtains module bond wire fatigue information by analyzing the harmonics of IGBT collector-emitter voltage, which is a method that can be applied online. However, the bond wire fatigue information is not amplified and is highly susceptible to interference. References [23], [24], [25] utilize the influence of bond wire fatigue on the IGBT's IV characteristic curve to achieve online detection of module bond wire fatigue. The methods are simple to implement in engineering and has high sensitivity. However, like the methods mentioned in the references above, it is affected by various factors such as junction temperature, bus voltage, and collector current.

In order to eliminate or reduce the influencing factors, [26], [27], [28] propose many detection methods for bond wire fatigue based on multidimensional detection parameters. Unfortunately, these methods either cannot remove the key influencing factor of junction temperature, or online detection is difficult to achieve. Consequently, this paper proposes a method for bond wire fatigue monitoring based on the K factor parameter. Firstly, the paper analyzes the generation mechanisms of the collector-emitter voltage spike and the auxiliary emitter-emitter voltage spike during the turn off process, as well as their relationship with junction temperature and bond wire fatigue. Secondly, the ratio of collector-emitter voltage spike to auxiliary emitter-emitter current spike, named the K factor, has been proposed as a detection parameter for bond wire fatigue in IGBT module. It is worth noting that the K factor is not influenced by operating parameters such as junction temperature and collector current in power electronic converter. This provides convenience for subsequent online monitoring. Furthermore, online monitoring of the K factor and the auxiliary emitter-emitter voltage spike has been implemented on a power electronic converter.

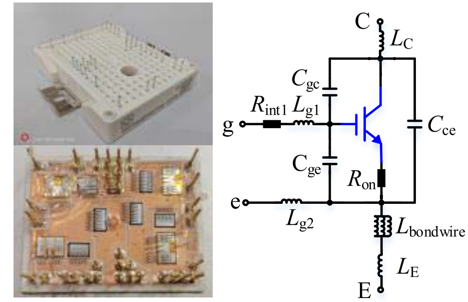

FIGURE 1. SRE100N065FSUT1M2 and its equivalent circuit.

II. THE *K* FACTOR AND THE MECHANISM OF VOLTAGE SPIKE DURING IGBT TURN-OFF PROCESS

This section provides a detailed analysis of the mechanism of voltage spikes generated by the collector emitter terminal and the auxiliary emitter-emitter terminal during the IGBT turn off process, and proposes a characterization parameter K factor for detecting module bond wire fatigue based on these voltage spikes. In addition, based on semiconductor physics, the reliability factors such as junction temperature and bond wire fatigue, as well as the impact of changes in operating conditions on voltage spikes, were explained in detail.

SRE100N065FSUT1M2 is a typical Easy2B packaged IGBT module. Fig. 1 shows the appearance, internal chip layout, and equivalent circuit model of the module. In the equivalent circuit, C_{ge}, C_{gc}, and C_{ce} are the equivalent capacitance of the IGBT, L_{g1}, L_{g2}, and R_{int1} are the equivalent inductances and resistance of the copper cladding and wire in the gate circuit, L_C and L_E are the equivalent inductance of the copper cladding in the power circuit and $L_{bondwire}$ is the equivalent inductance of the bond wire between the IGBT chip and the copper cladding.

A. THE MECHANISM OF VOLTAGE SPIKE DURING IGBT TURN-OFF PROCESS

The switching performance of IGBT can be obtained from the IGBT double pulse testing circuit shown in Fig. 2.

The double pulse test circuit in Fig. 2 comprises the under test IGBT in the green box and the freewheeling diode (FWD), the load inductance L_{load}, the DC power supply V_{dc}, and the pulse drive power supply V_{pulse} that drives the IGBT. In addition, the parasitic inductance of the DC bus capacitor and the line parasitic inductance are also shown in the figure, represented by L_{s1} and L_{s2}. Prior the IGBT turn off process commencing, the collector current I_C of the under test IGBT is consistent with the load current I_L. When the IGBT starts entering turn off process, due to the reversal of the gate driving power V_{pulse}, the direction of the gate current I_g is as shown in Fig. 2. Subsequently, the gate voltage V_{ge}, collector current I_C, collector emitter voltage V_{CE}, and auxiliary emitter-emitter voltage V_{eE} will vary according to their respective laws during the IGBT turn off process.

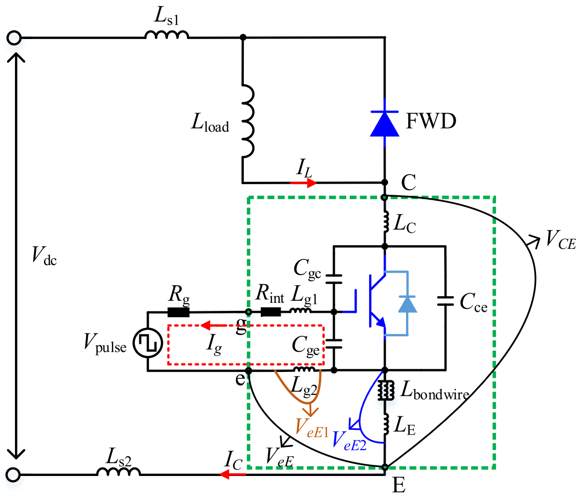

FIGURE 2. IGBT double pulse testing circuit.

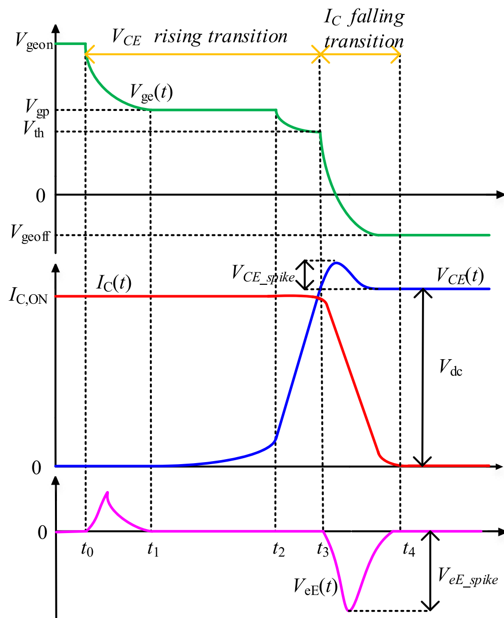

FIGURE 3. IGBT turn off process with inductive load.

The IGBT turn off process can be divided into two major steps [29], [30]. The Fig. 3 shows the waveforms of gate voltage V_{ge}, collector emitter voltage V_{CE}, collector current I_C, and auxiliary emitter-emitter voltage V_{eE} during the IGBT turn off process.

The main feature of the first step is that the collector emitter voltage V_{CE} rises to the bus voltage V_{dc}. In this step, due to the release of charges stored in the accumulation layer and N-type drift region, the collector current I_C can maintain its original value unchanged. When gate voltage V_{ge} falls from the gate drive voltage V_{geon} to the miller platform voltage V_{gp}, the gate capacitor C_{ge} acts as a power source to discharge the gate circuit and gate current I_g rapidly reverse increases to form overcurrent and then decreases to the steady-state value. At this stage, the rapidly changing gate current I_g generates inductance voltage V_{eE1} on the parasitic inductance L_{g2}. As the collector current I_C remains constant, no voltage is generated on the parasitic inductance $L_{bondwire}$ and L_E. Therefore, the auxiliary emitter-emitter voltage V_{eE} is equal to the inductance voltage V_{eE1} on L_{g2}.

The main feature of the second step is that the collector current I_C falls to zero. In this step, the gate voltage V_{ge} has dropped below the threshold voltage V_{th}, and the MOS channel is closed [29]. However, there is still excess storage charge to be consumed in the N-type drift region. Therefore, the falling process of collector current I_C in this step can be divided into two stages. In the first stage, some holes in the N-type drift region enter the P-well through the space charge region and are then swept out by the emitter. In the second stage, the remaining holes in the N-type drift region are consumed by the recombination mechanism. The disappearance of MOS channels causes the gate current I_g to approach zero, and the equivalent inductance L_{g2} of the gate circuit no longer generates inductance voltage. The falling of collector current I_C causes a large inductance voltage V_{eE2} to be generated by the parasitic inductance $L_{bondwire}$ of the bond wire and the copper cladding inductance L_E. Therefore, the auxiliary emitter-emitter voltage V_{eE} is equal to V_{eE2}.

At this point, due to the load current I_L flowing between the load inductor L_{load} and the FWD, the falling of collector current I_C causes the voltage spikes on the parasitic inductances L_{s1} and L_{s2} of the external line and DC bus capacitor. This voltage spike is applied to the collector C terminal and emitter E terminal of the IGBT, generating a large peak voltage V_{CE_peak}.

In summary, during the collector current I_C falling stage, the collector-emitter voltage peak V_{CE_peak} and the auxiliary emitter-emitter voltage spike V_{eE_spike} can be expressed by (1).

$$\begin{cases} V_{CE_peak} = V_{CE_spike} + V_{dc} = (L_{s1} + L_{s2}) \cdot \left.\frac{dI_C}{dt}\right|_{\max} + V_{dc} \\ V_{eE_spike} = -(L_E + L_{bondwire}) \cdot \left.\frac{dI_C}{dt}\right|_{\max} \end{cases} \tag{1}$$

From (1), it can be seen that the collector-emitter voltage peak V_{CE_peak} is formed by DC bus voltage V_{dc} and collector emitter voltage spike V_{CE_spike}, as shown in Fig. 3.

B. THE BOND WIRE FATIGUE CHARACTERIZATION PARAMETER K FACTOR

The mechanism of the generation of V_{CE_peak} and V_{eE_spike} during the falling stage of collector current I_C during the IGBT turn off process has been clearly explained. From (1), it can be seen that the voltage spikes generated at the collector-emitter terminal and the auxiliary emitter-emitter terminal are directly related to the parasitic inductance and the maximum rate of change of collector current.

Since the maximum change rate of collector current is affected by the factors such as junction temperature T_j, DC bus voltage V_{dc}, collector current I_C, and bond wire fatigue, both the collector-emitter voltage spike and the auxiliary emitter-emitter voltage spike are affected by the above

factors. A method that can eliminate or reduce the impact of the aforementioned factors on the fatigue characteristic parameters of the bond wire is desired. Utilizing the characteristic that both the collector-emitter voltage spike V_{CE_spike} and the auxiliary emitter-emitter voltage spike V_{eE_spike} reflects the maximum rate of change of collector current, the bond wire fatigue characterization parameter K factor is proposed. This can be expressed as follows.

$$K = \left|\frac{V_{CE_spike}}{V_{eE_spike}}\right| = \frac{(L_{s1} + L_{s2})}{(L_E + L_{bondwire})} \tag{2}$$

From (2), the K factor is only related to the parameters of parasitic inductance, and has nothing to do with junction temperature T_j, DC bus voltage V_{dc}, and collector current I_C. Interestingly, the change in parasitic inductance caused by module bond wire fatigue can be reflected in the K factor. After the above simple analysis, if the physical structure of the IGBT module other than the bond wire is intact, namely, the parasitic inductances L_{s1}, L_{s2}, and L_E do not change, the K factor can be used to accurately obtain the current bond wire fatigue information of the IGBT without being affected by other factors. This provides great convenience for distinguishing the junction temperature T_j and bond wire fatigue of IGBTs.

C. THE MAXIMUM RATE OF CHANGE OF COLLECTOR CURRENT IN COLLECTOR CURRENT FALLING STAGE

The collector-emitter voltage peak V_{CE_peak} and the auxiliary emitter-emitter voltage spike V_{eE_spike} is affected by multiple factors. It is known that these influencing factors all cause changes in the voltage spikes by affecting the maximum rate of change of collector current. The low doping concentration and larger width allow the N-type drift region to store a significant amount of holes during the IGBT on-state, and the consumption process of these stored holes determines the maximum rate of change of collector current. It should be note that during the collector current falling stage, the consumption of remaining holes in the N-type drift region within the IGBT undergoes two steps, corresponding to two charge consumption mechanisms: one is charge control principle and the other is recombination. Both of them have an impact on the maximum rate of change of collector current.

The consumption of remaining holes within the N-type drift region (N-doped region) and the expansion of the space charge region (Depletion layer) are shown in Fig. 4.

The collector current density J_{C1} during the first step of collector current falling stage can be expressed as follows [30].

$$J_{C1}(t) = a \cdot b \cdot \left(\frac{a \cdot b}{J_{C,ON}} + 4D_a \cdot t\right)^{-\frac{1}{2}} \tag{3}$$

In (3), a and b can be expressed as follows.

$$\begin{cases} a = \frac{\mu_n + \mu_p}{\mu_n} \\ b = q \cdot D_a \cdot 2p_0 \end{cases} \tag{4}$$

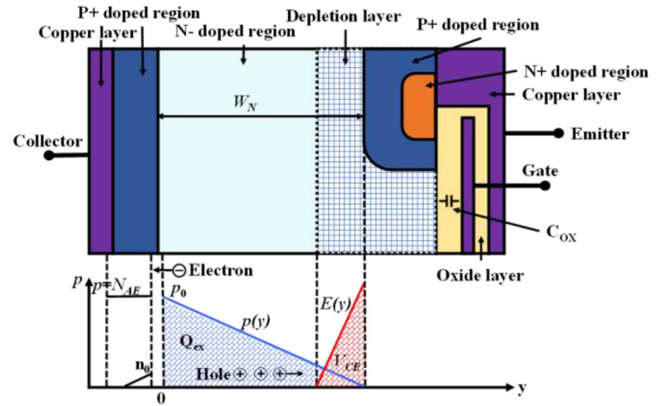

FIGURE 4. The consumption of remaining holes during the collector current falling stage.

In (4), μ_n, μ_p, is the electron and hole mobility; p_0 is the hole concentration during the IGBT on-state process; q is the unit charge; D_a is the bipolar diffusion coefficient; $J_{C,ON}$ is the current density during the IGBT on-state.

The collector current density J_{C2} during the second step of collector current falling stage can be expressed as follows [30].

$$J_{C2}(t) = J_{C,SS} \cdot \exp\left(-\frac{2t}{\tau_{HL}}\right) = \frac{q \cdot D_{nE} \cdot p_0^2}{L_{nE} \cdot N_{AE}} \cdot \exp\left(-\frac{2t}{\tau_{HL}}\right) \tag{5}$$

In (5), D_{nE} and L_{nE} are the diffusion coefficients and diffusion lengths of electrons in the P+ collector region, respectively; N_{AE} is the doping concentration in the P+ collector region; τ_{HL} is the carrier lifetime in the N-type base region under high injection conditions; $J_{C,SS}$ is the initial current of the second step.

J_{C1} and J_{C2} represent two steps of the collector current falling stage. By simultaneously taking the derivatives of both J_{C1} and J_{C2}, the maximum rate of change of collector current can be determined as the greater of the two resulting values. This can be expressed as follows.

$$\left.\frac{dI_C}{dt}\right|_{\max} = \max\left(A \cdot \left|\frac{d[J_{C1}(t)]}{dt}\right|_{t=0}, A \cdot \left|\frac{d[J_{C2}(t)]}{dt}\right|_{t=0}\right) \tag{6}$$

In (5), A is the active area. The maximum rate of change in collector current density for each step during the collector current falling stage can be expressed as follows.

$$\begin{cases} \left|\frac{d[J_{C1}(t)]}{dt}\right|_{t=0} = \left|4D_a \cdot \left(J_{C,ON}\right)^{\frac{3}{2}} \cdot (a \cdot b)^{-\frac{1}{2}}\right| \\ \left|\frac{d[J_{C2}(t)]}{dt}\right|_{t=0} = \left|\frac{2q \cdot D_{nE} \cdot p_0^2}{L_{nE} \cdot N_{AE} \cdot \tau_{HL}}\right| \end{cases} \tag{7}$$

D. ANALYSIS OF THE FACTORS AFFECTING VOLTAGE SPIKES

The junction temperature T_j, bond wire fatigue, and IGBT operating parameters can all affect the collector emitter voltage spike V_{CE_peak} and the auxiliary emitter-emitter voltage spike V_{eE_spike}, but the ways of influence are different. Fig. 5 shows the dependency details of junction

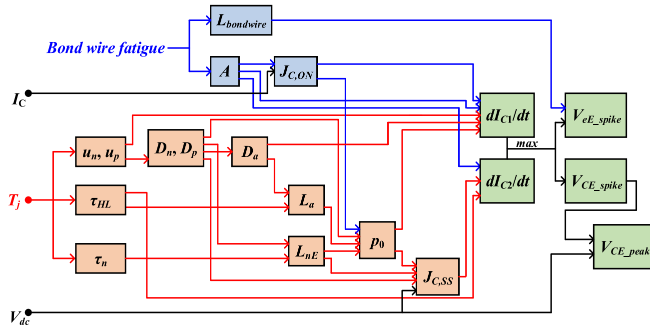

FIGURE 5. The dependency details of the voltage spikes.

temperature T_{j}, bond wire fatigue, DC bus voltage V_{dc}, and collector current I_C on voltage spikes.

The parameters μ_n, μ_p, D_{nE}, L_{nE}, D_a, τ_n, τ_{HL} and $J_{C,SS}$ are the physical parameters of the semiconductor and are all functions of the junction temperature T_{j}. The reference [30] gives the functional relationship between these parameters and the junction temperature T_{j}. After comprehensive analysis, it is found that the maximum rate of change of collector current decreases with the increase of the junction temperature T_{j}, showing a negative correlation.

For bond wire fatigue, assuming that the DC bus voltage V_{dc} and collector current I_C remain constant, the decrease in active area A will lead to an increase in $J_{C,ON}$, which will result in the maximum rate of change of collector current being minimally affected by bond wire fatigue. However, due to the parasitic inductance $L_{bondwire}$, it directly affects the magnitude of the auxiliary emitter-emitter voltage spike V_{eE_spike}.

III. IGBT JUNCTION TEMPERATURE AND BOND WIRE FATIGUE EXTRACTION METHOD

This section proposes a method based on the K factor to distinguish between IGBT junction temperature and bond wire fatigue by utilizing the bond wire fatigue model of V_{eE_spike}.

A. THE BOND WIRE FATIGUE MODEL OF VEE_SPIKE

Assuming that the parasitic inductance of a single bond wire is defined as L_{bs}, and the remaining number of bond wires is defined as $n_{bondwire}$, and the total number of bond wires is defined as n_{total}. The bond wire in the module are composed of multiple bond wires in parallel, so the parasitic inductance of bond wire can be calculated as $L_{bondwire}$=L_{bs}/$n_{bondwire}$.

According to (1), the auxiliary emitter-emitter voltage spike V_{eE_spike} model without considering bond wire fatigue is as follows.

$$V_{eE_spike} = \left(L_E + \frac{L_{bs}}{n_{total}}\right) \cdot \left.\frac{dI_C}{dt}\right|_{\max} \tag{8}$$

Taking (8) as an example, the model of V_{eE_spike} under different deepening of bond wire fatigue as follows.

$$V_{eE_spike}\big|_{bondwirefatigue} = \left(L_E + \frac{L_{bs}}{n_{bondwire}}\right) \cdot \left.\frac{dI_C}{dt}\right|_{\max} \tag{9}$$

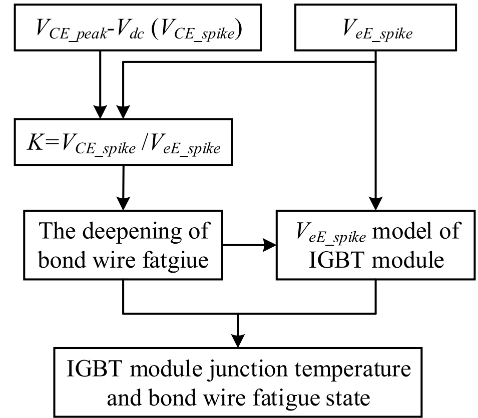

FIGURE 6. Distinguishing method process.

To describe the V_{eE_spike} model with bond wire fatigue using the V_{eE_spike} model without bond wire fatigue given by (8), and to reflect the bond wire fatigue state, the simplified bond wire fatigue model based on (8) and (9) is as follows.

$$\begin{aligned}\frac{V_{eE_spike}\big|_{bondwirefatigue}}{V_{eE_spike}} &= \frac{n_{total}}{n_{bondwire}} \cdot \frac{L_E \cdot n_{bondwire} + L_{bs}}{L_E \cdot n_{total} + L_{bs}} \\ &= \frac{n_{total}}{n_{bondwire}} \cdot \frac{1}{A_{JX}}\end{aligned} \tag{10}$$

In (10), A_{JX} is referred to as the correction coefficient. It can be seen that A_{JX} is related to n_{total} and $n_{bondwire}$. When $n_{bondwire}$=n_{total}, A_{JX}=1. As the bond wire fatigue deepening, $n_{bondwire}$<n_{total}, A_{JX}>1.

B. DISTINGUISHING METHOD BASED ON K-FACTOR AND VEE_SPIKE MODEL

The distinguishing process is shown in Fig. 6.

From Fig. 6, the K factor is utilized to obtain the current bond wire fatigue state of the IGBT module. Subsequently, based on a model of V_{eE_spike} that takes into account the junction temperature T_{j}, bond wire fatigue, and collector current I_C, the current junction temperature of the IGBT under test is obtained.

It should be noted that only when the load current I_L flows through the IGBT can be referred to as the collector current I_C.

IV. EXPERIMENTAL VERIFICATION

This section tests IGBT's dynamic characteristics using a double pulse testing circuit, as shown in Fig. 2. The theoretical analysis mentioned above has been validated through experimental data, and a model for the K factor and V_{eE_spike} has been constructed. Additionally, in this section, the bond wire fatigue was simulated by the number of cutting bond wires.

A. EXPERIMENTAL CONDITIONS AND PLATFORM

In order to obtain the corresponding experimental data and validate the theoretical analysis mentioned above, the IGBT

FIGURE 7. IGBT dynamic characteristics testing platform (left) and power cycling platform (right).

TABLE 1. Test conditions.

Parameter	Value	Parameter	Value
Diver Resistor	10Ω	Load Inductor	110uF
Diver Voltage	+15/-8V	Bus Capacitor	1760uF
DC Voltage	425V	Junction Temperature	30°C-130°C
Load Current	30A-90A	Number of bond wire fatigue	2、3、4

module dynamic characteristic testing platform was used to test and analyze the module under test. The IGBT dynamic characteristic testing platform is shown on the left in Fig. 7.

The testing conditions for the IGBT module are shown in Table 1.

The IGBT module used is the SRE100N065FSUT1M2 series packaged in Easy2B. The number of cutting bond wires between the IGBT chip and the copper substrate represents the fatigue levels as follows: Fatigue1 corresponds to cutting 2 bond wires, Fatigue2 corresponds to cutting 3 bond wires, and Fatigue3 indicates cutting 4 bond wires.

B. EXPERIMENTAL RESULT

This part validates the effect of IGBT module collector current I_C, junction temperature T_j, and bond wire fatigue on the waveforms of V_{CE} and V_{eE} in the IGBT turn off process.

Firstly, according to (7) and Fig. 5, it can be concluded that an increase in collector current density $J_{C,ON}$ of the IGBT on-state the leads to an increase in the maximum rate of change of the collector current, as evidenced by the dependence on the influencing factors. The increase in collector current I_C leads to an increase in collector current density $J_{C,ON}$ under the condition that the active area A remains unchanged. So, it can be concluded that the maximum rate of change of collector current will increase with an increase in collector current I_C, which is experimentally verified in Fig. 8. The aforementioned experiment was conducted under the conditions of a healthy IGBT module and a junction temperature of 30°C.

Similarly, based on the dependency details of the relevant influencing factors in Fig. 5, the maximum rate of change of the collector current will decrease with increasing junction temperature T_j. Combining (1), it can be concluded that the collector emitter peak voltage V_{CE_peak} and the auxiliary emitter-emitter voltage spike V_{eE_spike} will decrease with increasing junction temperature T_j. Therefore, in order to verify the influence of junction temperature on V_{CE_peak} and V_{eE_spike}, testing was conducted on a healthy IGBT module under the condition of a collector current of 60A. The experimental waveforms are shown in Fig. 9.

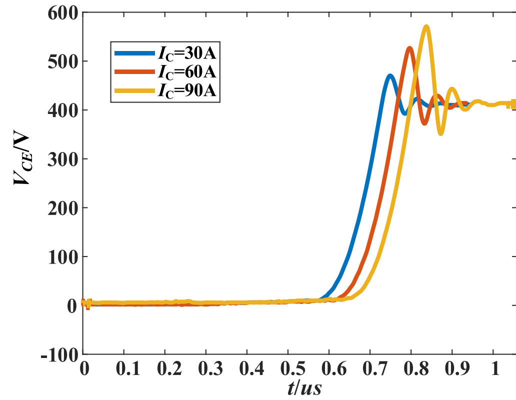

a. The waveform V_{CE} under different collector current I_C

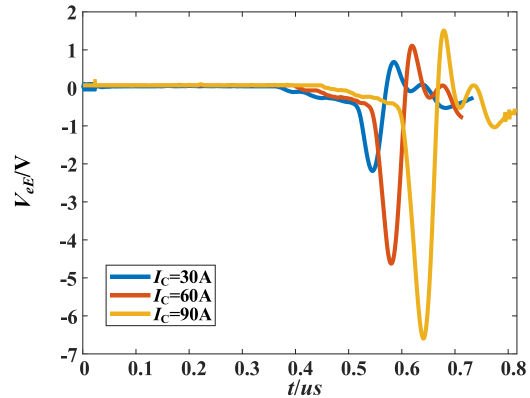

b. The waveform V_{eE} under different collector current I_C

FIGURE 8. The waveforms of V_{eE} and V_{CE} under different I_C.

The IGBT equivalent circuit model shown in Fig. 1 indicates that when the IGBT module experiences bond wire fatigue, the parasitic inductance parameters between the auxiliary emitter and emitter will undergo changes, leading to an increase in $L_{bondwire}$. Based on the analysis provided in the previous section, it can be inferred that the impact of bond wire fatigue on the maximum rate of change in collector current can be disregarded. Consequently, the variation of parasitic inductance is the main factor affecting voltage spikes.

In order to verify the influence of bond wire fatigue on V_{CE_peak} and V_{eE_spike}, the same IGBT module with different deepening of bond wire fatigue was tested under the conditions of a collector current of 60A and a junction temperature of 30°C. The experimental waveforms are shown in Fig. 10.

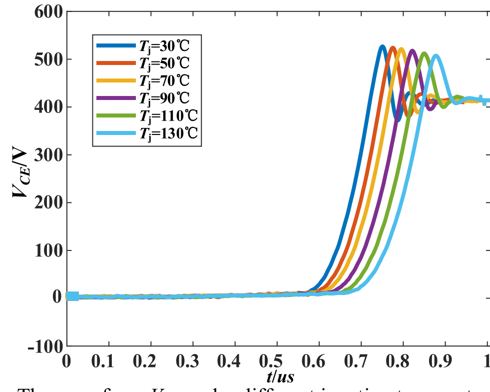

a.The waveform V_{CE} under different junction temperature T_j

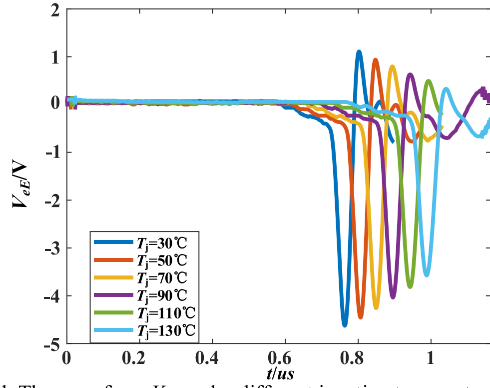

b.The waveform V_{eE} under different junction temperature T_j

FIGURE 9. The waveforms of V_{eE} and V_{CE} under different T_j.

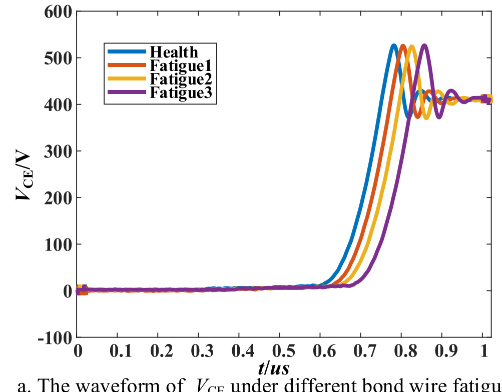

a. The waveform of V_{CE} under different bond wire fatigue

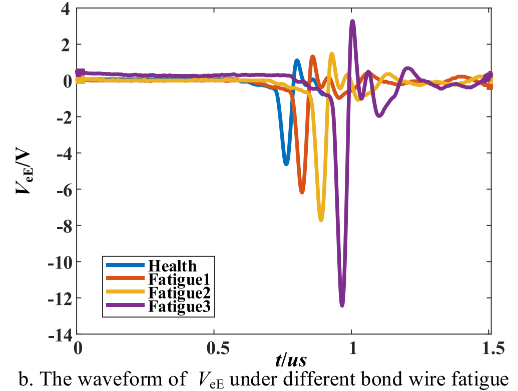

b. The waveform of V_{eE} under different bond wire fatigue

FIGURE 10. The waveforms of V_{eE} and V_{CE} under different bond wire fatigue.

Due to the minimal impact of bond wire fatigue on the maximum rate of change of collector current, V_{CE_peak} will be slightly affected by bond wire fatigue.

Consequently, the experimental results are basically consistent with the aforementioned analysis. It also provides convenience for constructing the model of junction temperature and bond wire fatigue based on the K factor and V_{eE_spike}.

C. VEE_SPIKE MODEL AND K FACTOR

In this part, the V_{eE_spike} model of bond wire fatigue and K-factor of the SRE100N065FSUT1M2 are established.

The waveform of V_{CE} with bond wire fatigue illustrates that V_{CE_peak} is minimally affected by bond wire fatigue. To further demonstrate this, the variation trends of V_{CE_peak} and bond wire fatigue under different conditions (junction temperature, collector current) are shown in Fig. 11.

It can be seen that the influence of bond wire fatigue on V_{CE_peak} can be ignored. In addition, the relationship between V_{CE_peak} and junction temperature T_j under different collector currents is shown by the dashed line in Fig. 12.

The solid line in Fig. 12 is the fitting result, so the V_{CE_peak} fitting model based on data acquisition is as follows.

$$V_{CE_peak} = -0.003 I_C \cdot T_j + 1.746 I_C + 425 \tag{11}$$

According to the relationship between V_{CE_peak} and V_{CE_spike} described in (1), combined with (11) and V_{dc}=425V in Table 1, the model of V_{CE_spike} as follows.

$$V_{CE_spike} = -0.003 I_C \cdot T_j + 1.746 I_C \tag{12}$$

The relationship of V_{eE_spike} and junction temperature T_j under different collector current I_C is shown by the dashed line in Fig. 13. As the junction temperature T_j increases, V_{eE_spike} decrease.

The solid line in Fig. 13 is the fitting result, so the V_{eE_spike} fitting model based on data acquisition is as follows.

$$V_{eE_spike} = -0.00013 I_C \cdot T_j + 0.078 I_C \tag{13}$$

The relationship of V_{eE_spike} and bond wire fatigue under different junction temperature T_j is shown in Fig. 14. As the bond wire fatigue deepening, V_{eE_spike} increases.

Since the number of bond wires to be tested for IGBTs in SRE100N065FSUT1M2 module is 5, the V_{eE_spike} simplified bond wire fatigue model for SRE100N065FSUT1M2 module is as follows using the V_{eE_spike} simplified bond wire fatigue model shown in (14).

$$V_{eE_spike}\big|_{bondwirefatigue} = V_{eE_spike} \cdot \frac{5}{n_{bondwire}} \cdot \frac{1}{A_{JX}} \tag{14}$$

Based on (2), (12), (13) and (14), the model for the K factor parameter under the experimental conditions was obtained, as follows.

$$K = \frac{V_{CE_spike}}{V_{eE_spike}\big|_{bondwirefatigue}} = 23 \cdot A_{JX} \cdot \frac{n_{bondwire}}{5} \tag{15}$$

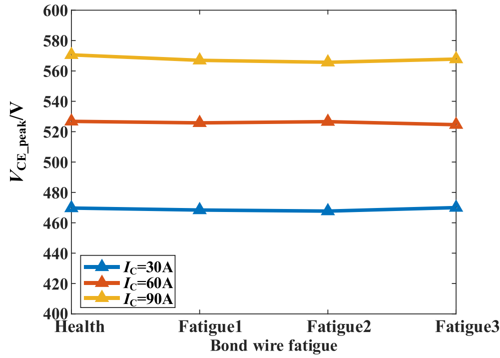

a. The relationship between V_{CE_peak} and bond wire fatigue under different collector current I_C

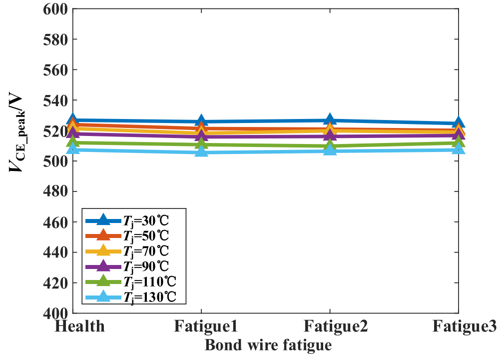

b. The relationship between V_{CE_peak} and bond wire fatigue under different junction temperature T_j

FIGURE 11. The relationship between V_{CE_peak} and bond wire fatigue under different conditions.

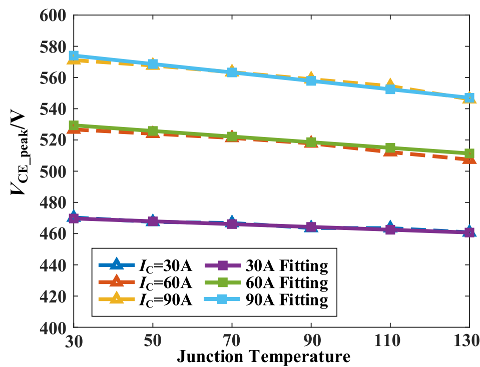

FIGURE 12. The relationship between V_{CE_peak} and junction temperature T_j under different collector current I_C.

As mentioned earlier, L_E is the parasitic inductance of the copper cladding that exists between the internal emitter terminal and the bond wire. In the SRE100N065FSUT1M2 module, this parasitic inductance does not differ significantly from the bond wire parasitic inductance in terms of orders of magnitude. Therefore, A_{JX} is approximately equal to 1, and we can set A_{JX} =1 in (15).

Based on this, the values of the K factor obtained through calculations based on the K factor model and actual measurements under different conditions are shown in Fig. 15.

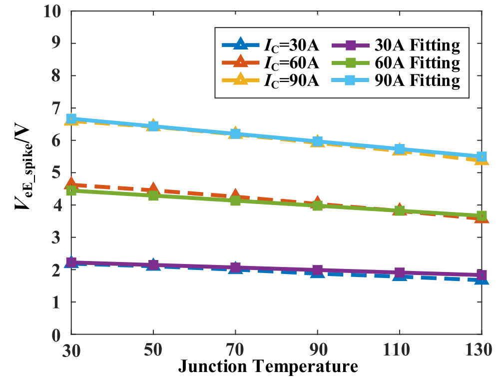

FIGURE 13. The relationship between V_{eE_spike} and junction temperature T_j under different collector current I_C.

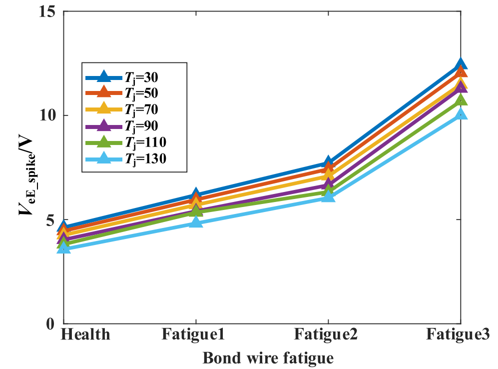

FIGURE 14. The relationship between V_{eE_spike} and bond wire fatigue under different junction temperature T_j.

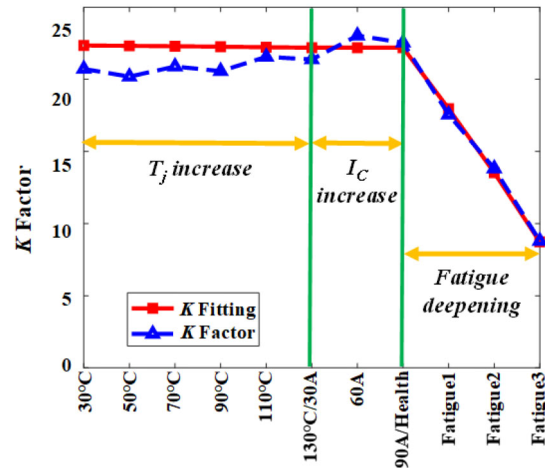

FIGURE 15. The trends in actual and fitting values of K factor under different conditions.

It can be seen that when the IGBT module does not incur bond wire fatigue, the actual K factor parameters do not exhibit a certain changing pattern with increasing junction temperature and collector current. Instead, it fluctuates around the fixed values provided by the K factor model. This is consistent with the previous analysis, which suggests that the K factor parameters are determined by the parasitic inductance parameters. However, due to bond wire fatigue

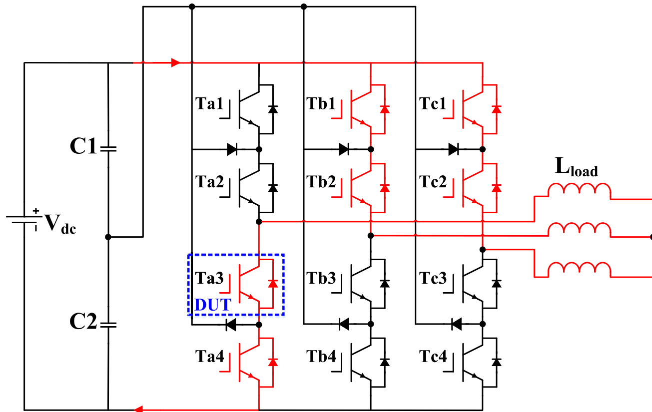

FIGURE 16. The position of DUT and effective commutation path.

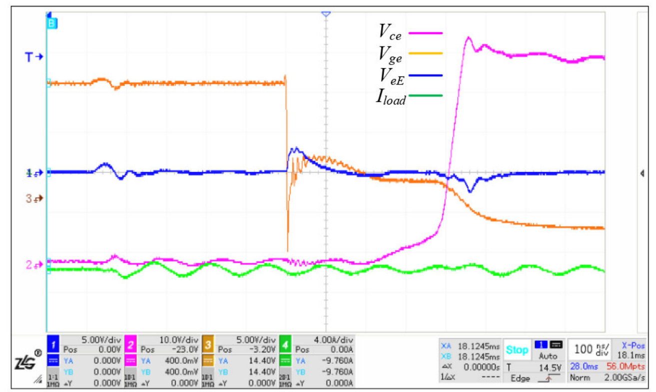

FIGURE 17. The turn off waveforms of the IGBT under test within the effective commutation path.

in the module, the parasitic inductance parameters undergo changes. As shown in Fig. 15, in the region of fatigue deepening, the K factor undergoes noticeable variations, and as the fatigue deepening, the K factor decreases.

V. IMPLEMENTATION OF ONLINE MONITORING

To obtain real-time information on junction temperature and bond wire fatigue in IGBT module, it is proposed to utilize an oscilloscope as the data acquisition device. This will be achieved by monitoring the junction temperature characterization parameter V_{eE_spike} and the bond wire fatigue characterization parameter K factor. The specific method has been illustrated in Fig. 6.

The oscilloscope is adjusted to automatic triggering mode to record the signals of load current I_{load}, V_{CE}, V_{ge} and V_{eE} with the IGBT. The triggering source is set as V_{eE}. When the signal triggers, the direction and magnitude of I_{load} are determined, and if the conditions are met, the K factor and V_{eE} will be outputted. The feasibility of online extraction of the K factor and V_{eE_spike} model scheme will be verified using a three phase power cycling platform, as shown in Fig. 7 (right).

The IGBT under test in the module is Ta3. Its position in the topology and the partially effective commutation paths that can be used for extracting the K factor and V_{eE_spike} are shown in Fig. 16.

The blue box in the Fig. 16 represents the IGBT under test, and the red line represents an effective commutation path that can be used to extract the K factor and V_{eE_spike} during the operation of the experimental platform.

The signal of the IGBT under test, collected by the oscilloscope, is shown in Fig. 17.

Continuous reading of data obtained from the oscilloscope enables online monitoring of the K factor and V_{eE_spike}. The variations of the K factor and t V_{eE_spike} are recorded when the load current was 30A and 60A, as shown in Fig. 18.

During the three phase power cycling platform, only the voltage spikes generated by the load current flowing through the tested IGBT can reflect the state of bond wire fatigue and junction temperature. Only in this way can we obtain

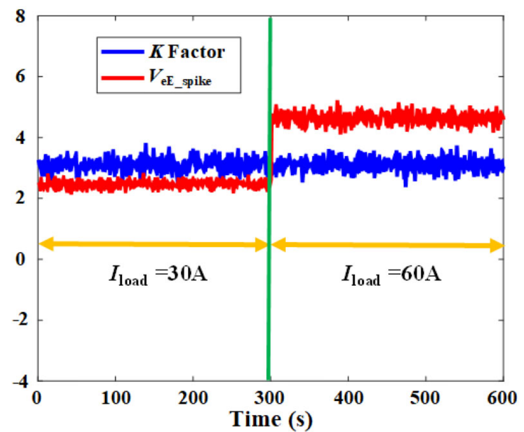

FIGURE 18. Online monitoring data for the K factor and V_{eE_spike}.

the K factor and V_{eE_spike} is correct, while the opposite is incorrect.

Under the conditions of load currents of 30A and 60A, the K factor parameter remains relatively constant in the Fig. 19, which is consistent with the previous theoretical analysis. It should be noted that the parameter value of the K factor is approximately around 3.1, which differs significantly from the parameter value in the previous K factor model. This discrepancy is due to the inconsistent external parasitic inductance parameters between the three-phase reactive power inverter and the dynamic characteristic test platform. Additionally, in order to suppress voltage spikes, the three phase power cycling platform has added absorbent capacitors at the IGBT module, which further reduces the voltage spikes and leads to inconsistencies in the K factor parameter values. Furthermore, V_{eE_spike} increases with the increase in load current, which is consistent with the previous experimental results.

VI. CONCLUSION

The proposed approach in this paper utilizes the K factor as a monitoring parameter for IGBT module bond wire fatigue. This parameter is not affected by junction temperature, DC bus voltage, collector current, or load current. Building upon

this, the bond wire fatigue state obtained using the K factor is combined with the V_{eE_spike} model of bond wire fatigue can extract the junction temperature of IGBT modules. It should be noted that when obtaining the value of K factor based on the SRE100N065FSUT1M2 module using $A_{JX}=1$, there may be deviations in the bond wire fatigue status determination when L_E is much larger than $L_{bondwire}$. Therefore, it is necessary to adjust A_{JX} based on the actual conditions of the module's L_E.

Applying this method requires attention to two conditions. Firstly, it is necessary to ensure that the bond wire is located between the internal auxiliary emitter and emitter terminal of the IGBT module. Secondly, changes in the external parasitic parameters of the IGBT module need to be taken into account. These two conditions need to be met simultaneously, otherwise it will cause the method to fail.

REFERENCES

[1] U. Choi, F. Blaabjerg, and K. Lee, "Study and handling methods of power IGBT module failures in power electronic converter systems," *IEEE Trans. Power Electron.*, vol. 30, no. 5, pp. 2517–2533, May 2015, doi: 10.1109/TPEL.2014.2373390.

[2] Q. Li et al., "Review of the failure mechanism and methodologies of IGBT bonding wire," *IEEE Trans. Compon., Packag. Manuf. Technol.*, vol. 13, no. 7, pp. 1045–1057, Jul. 2023, doi: 10.1109/TCPMT.2023.3297224.

[3] M. A. Eleffendi and C. M. Johnson, "In-service diagnostics for wire-bond lift-off and solder fatigue of power semiconductor packages," *IEEE Trans. Power Electron.*, vol. 32, no. 9, pp. 7187–7198, Sep. 2017, doi: 10.1109/TPEL.2016.2628705.

[4] H. Wang et al., "Transitioning to physics-of-failure as a reliability driver in power electronics," *IEEE J. Emerg. Sel. Topics Power Electron.*, vol. 2, no. 1, pp. 97–114, Mar. 2014, doi: 10.1109/JESTPE.2013.2290282.

[5] H. Fu et al., "Failure mechanism analysis of bond wire of high power IGBT under different load current," in *Proc. IEEE 5th Int. Electr. Energy Conf. (CIEEC)*, Nangjing, China, 2022, pp. 798–803.

[6] C. Tu, H. Xu, B. Xiao, J. Lu, Q. Guo, and L. Long, "Research on the influence of bond wire lift-off position on the electro-thermal characteristics of IGBT," *IEEE Trans. Electron Devices*, vol. 69, no. 3, pp. 1271–1278, Mar. 2022, doi: 10.1109/TED.2022.3140689.

[7] X. Chai et al., "Online junction temperature measurement of double-sided cooling IGBT power module through on-state voltage with high current," *Chin. J. Electr. Eng.*, vol. 8, no. 4, pp. 104–112, Dec. 2022, doi: 10.23919/CJEE.2022.000042.

[8] W. Kexin, D. Mingxing, X. Linlin, and L. Jian, "Study of bonding wire failure effects on external measurable signals of IGBT module," *IEEE Trans. Device Mater. Rel.*, vol. 14, no. 1, pp. 83–89, Mar. 2014, doi: 10.1109/TDMR.2012.2200485.

[9] S. Das, F. Khan, M. K. Alam, and P. Goli, "Detection of aging related IGBT bond-wire lift-off using spread spectrum time domain reflectometry (SSTDR)," in *Proc. IEEE Appl. Power Electron. Conf. Expos. (APEC)*, Tampa, FL, USA, 2017, pp. 789–794.

[10] A. Hanif, J. Major, D. DeVoto, and F. Khan, "Bond wire damage detection and state of health estimation of a 1200V, 900A dual pack IGBT power module using the RL-equivalent circuit," in *Proc. IEEE Appl. Power Electron. Conf. Expos. (APEC)*, Anaheim, CA, USA, 2019, pp. 3421–4326.

[11] A. Hanif, D. DeVoto, and F. Khan, "Bond wire damage detection and SOH estimation of a dual-pack IGBT power module using active power cycling and reflectometry," *IEEE Trans. Power Electron.*, vol. 35, no. 7, pp. 6761–6772, Jul. 2020, doi: 10.1109/TPEL.2019.2958898.

[12] A. Hanif, A. N. M. Wasekul Azad, and F. Khan, "Detection of bond wire lift off in IGBT power modules using ultrasound resonators," in *Proc. IEEE Appl. Power Electron. Conf. Expos. (APEC)*, New Orleans, LA, USA, 2020, pp. 345–350.

[13] M. Du, K. Wei, J. Li, and L. Xie, "Condition monitoring IGBT module bond wire lift-off using measurable signals," in *Proc. 7th Int. Power Electron. Motion Control Conf.*, Harbin, China, 2012, pp. 1492–1496.

[14] S. Zhou, L. Zhou, and P. Sun, "Monitoring potential defects in an IGBT module based on dynamic changes of the gate current," *IEEE Trans. Power Electron.*, vol. 28, no. 3, pp. 1479–1487, Mar. 2013, doi: 10.1109/TPEL.2012.2210249.

[15] K. Wang, L. Zhou, P. Sun, and X. Du, "Monitoring bond wires fatigue of multichip IGBT module using time duration of the gate charge," *IEEE Trans. Power Electron.*, vol. 36, no. 1, pp. 888–897, Jan. 2021, doi: 10.1109/TPEL.2020.3005183.

[16] Y. Yang and P. Zhang, "A novel bond wire fault detection method for IGBT modules based on turn-on gate voltage overshoot," *IEEE Trans. Power Electron.*, vol. 36, no. 7, pp. 7501–7512, Jul. 2021, doi: 10.1109/TPEL.2020.3047135.

[17] Y. Peng, L. Zhou, X. Du, P. Sun, and K. Wang. "Junction temperature estimation of IGBT module via a bond wires lift-off independent parameter VgE-np," *IET. Power Electron.*, vol. 11, no. 2, pp. 320–328, Jul. 2021, doi: 10.1049/IET-PEL.2017.0168.

[18] L. Jing, M. Du, K. Wei, and W. G. Hurley, "A health monitoring method for bond wires in IGBT modules based on voltage ringing characteristics," *IEEE Trans. Electron Devices*, vol. 66, no. 9, pp. 3953–3960, Sep. 2019, doi: 10.1109/TED.2019.2931445.

[19] W. Zhang et al., "In Situ Diagnosis of multichip IGBT module wire bonding faults based on collector voltage undershoot," *IEEE Trans. Ind. Electron.*, vol. 70, no. 3, pp. 3045–3054, Mar. 2023, doi: 10.1109/TIE.2022.3172768.

[20] Y. Peng, P. Sun, L. Zhou, X. Du, and J. Cai, "A temperature-independent method for monitoring the degradation of bond wires in IGBT modules based on transfer characteristics," in *Proc. IEEE Appl. Power Electron. Conf. Expos. (APEC)*, Tampa, FL, USA, 2017, pp. 751–755.

[21] P. Sun, C. Gong, X. Du, Y. Peng, B. Wang, and L. Zhou, "Condition monitoring IGBT module bond wires fatigue using short-circuit current identification," *IEEE Trans. Power Electron.*, vol. 32, no. 5, pp. 3777–3786, May 2017, doi: 10.1109/TPEL.2016.2585669.

[22] F. Yüce and M. Hiller, "Investigation of bond wire lift-off by analyzing the controller output voltage harmonics for the purpose of condition monitoring," in *Proc. 22nd Eur. Conf. Power Electron. Appl.*, Lyon, France, 2020, pp. P.1–P.10.

[23] A. Singh, A. Anurag, and S. Anand, "Evaluation of Vce at inflection point for monitoring bond wire degradation in discrete packaged IGBTs," *IEEE Trans. Power Electron.*, vol. 32, no. 4, pp. 2481–2484, Apr. 2017, doi: 10.1109/TPEL.2016.2621757.

[24] V. Smet, F. Forest, J.-J. Huselstein, A. Rashed, and F. Richardeau, "Evaluation of Vce monitoring as a real-time method to estimate aging of bond wire-IGBT modules stressed by power cycling," *IEEE Trans. Ind. Electron.*, vol. 60, no. 7, pp. 2760–2770, Jul. 2013, doi: 10.1109/TIE.2012.2196894.

[25] S. Liu, C. Tu, L. Long, H. Xu, B. Xiao, and Z. Zhu, "A method monitoring healthy state of bond wires in IGBT based on dV_{CE}/di_C," in *Proc. 48th Annu. Conf. IEEE Ind. Electron. Soc.*, Brussels, Belgium, 2022, pp. 1–6.

[26] J. Luo et al., "A thermal-mechanical deformation based fault diagnosis method utilizing support vector machine algorithm for IGBT bonding wire crack detection," in *Proc. CAA Symp. Fault Detect., Superv., Saf. Techn. Processes (SAFEPROCESS)*, Chengdu, China, 2021, pp. 1–4.

[27] Y. Li et al., "A multi-parameter condition monitoring method for IGBT bond wire," in *Proc. IEEE 5th Int. Electr. Energy Conf. (CIEEC)*, Nangjing, China, 2022, pp. 776–781.

[28] Y. Yang, X. Ding, and P. Zhang, "A novel junction temperature estimation method independent of bond wire degradation for IGBT," *IEEE Trans. Power Electron.*, vol. 38, no. 8, pp. 10256–10268, Aug. 2023, doi: 10.1109/TPEL.2023.3274126.

[29] H. Luo, Y. Chen, P. Sun, W. Li, and X. He, "Junction temperature extraction approach with turn-off delay time for high-voltage high-power IGBT modules," *IEEE Trans. Power Electron.*, vol. 31, no. 7, pp. 5122–5132, Jul. 2016, doi: 10.1109/TPEL.2015.2481465

[30] Y. Chen, H. Luo, W. Li, X. He, F. Iannuzzo, and F. Blaabjerg, "Analytical and experimental investigation on a dynamic thermo-sensitive electrical parameter with maximum di_C/dt during turn-off for high power trench gate/field-stop IGBT modules," *IEEE Trans. Power Electron.*, vol. 32, no. 8, pp. 6394–6404, Aug. 2017, doi: 10.1109/TPEL.2016.2619620.